# TiC Nanocrystal Formation from Carburization of Laser-Grown Ti/O/C Nanopowders for Nanostructured Ceramics

**Y. Leconte,[†] H. Maskrot,[†] N. Herlin-Boime,*[,†] D. Porterat,[†] C. Reynaud,[†] S. Gierlotka,[‡] A. Swiderska-Sroda,[‡] and J. Vicens[§]**

*Laboratoire Francis Perrin (CEA-CNRS URA 2453), Service des Photons, Atomes et Molécules, DSM/DRECAM, CEA-Saclay, 91191 Gif sur Yvette Cedex, France, Institut of High-Pressure Physics, Polish Academy of Sciences, Sokolowska 29/37, 01-142 Warsaw, Poland, and SIFCOM-ENSICAEN, 6 boulevard du maréchal Juin, 14050 Caen Cedex, France*

*Received: August 10, 2005; In Final Form: October 17, 2005*

Refractory carbide ceramics (TiC and ZrC) raise interest as promising materials for high-temperature applications such as structural materials for the future generation of nuclear reactors. In this context, nanostructured ceramics are expected to exhibit improved thermomechanical properties as well as better behavior under irradiation when compared to conventional materials. It is therefore necessary to synthesize carbide nanocrystals of such materials to elaborate the ceramics. We report here the formation study of TiC nanocrystals through the direct carburization of Ti/O/C nanopowders grown by laser pyrolysis. A spray of titanium tetraisopropoxide was laser pyrolyzed with ethylene as the sensitizer, leading to Ti/O/C nanopowders with various C contents controlled by the synthesis conditions. Annealing treatments performed on these nanopowders under an inert atmosphere without any C addition enabled the formation of TiC grains through the carburization of the oxide phase by free C incorporated during the synthesis. The powders were characterized by X-ray diffraction, scanning electron microscopy, and transmission electron microscopy. The final TiC grain size was about 80 nm, and the grains were monocrystalline. The influence of the free C content on the grain growth during the annealing step, together with its effects on the densification of the ceramics after sintering by high-pressure flash sintering, was examined. A 93% densification was finally achieved.

## Introduction

Hard refractory carbides, and especially TiC, can be encountered through various applications: structure or coating material in cutting tools,[1] reinforcing component in oxide[2] or non-oxide[3,4] ceramics, hard alloys, etc. Over the past decade, the field of nanostructured composites has raised large interest because these materials provide a promising means to overcome the typical drawbacks of traditional ceramics exhibiting low ductility and high brittleness. The reinforcement of a composite by nanometric components can lead to an improvement of the performances of the obtained material, as can be seen in the case of SiC/TiC composites.[5,6] Moreover, nanostructured ceramics contain a very large amount of grain boundaries and are therefore assumed to allow a fast recovery of irradiation-induced defects.[7] This latter assumption, when confirmed, could pave the way to a large-scale employment of these kinds of materials in nuclear industry applications.[8]

A lot of techniques can be used to synthesize TiC powders. Among them can be found the pyrolysis or carbothermal reduction of alkoxides,[9] gaseous phase reaction or magnesium reduction of $TiCl_4$ and hydrocarbons,[10,11] thermal plasma,[12] mechanical alloying and direct reaction between Ti and C,[13] etc. The most commonly used method at an industrial scale is the carbothermal reduction of $TiO_2$ by carbon black. This reaction requires high temperatures (>1700 °C) and long reaction times (>10 h) because the contact area between the mixed $TiO_2$ and C raw particles is not very large.[14−16] An efficient way to lower the process temperature together with the TiC particle size is to decrease the $TiO_2$ particle size and to coat them with C. The reactivity between $TiO_2$ and C could then be enhanced.[17] Some authors have reported an efficient carbothermal reduction at a temperature as low as 1300 °C, starting from nanometric $TiO_2$ particles and coating them through the pyrolysis of propylene[18] or with methylcellulose.[19] Thus, it would be interesting to be able to synthesize in a one-step process the C-coated $TiO_2$ nanoparticles.

To produce nanoparticles on a large scale, the laser pyrolysis method offers several advantages. This latter technique, widely studied and developed for SiC synthesis from a silane + acetylene or ethylene mixture,[20,21] permits the elaboration of a large variety of products thanks to the numerous precursors that can be used. In the case of TiC, the laser pyrolysis of a mixture constituted by $TiCl_4$ + hydrocarbon ($C_2H_2$, $C_2H_4$, etc.) has already been reported,[22] but the use of this precursor can lead to pollution by Cl and produces corrosive species such as HCl during the synthesis. The carbothermal reduction, or carburization process, of $TiO_2$ + C nanocomposites allows the use of cheap alkoxide precursors containing only Ti, C, O, and H to synthesize the $TiO_2$/C mixture.

The densification of nanostructured ceramics is the subject of numerous studies: The point is to achieve the densification without igniting the grain growth.[7] In this context, an original flash-sintering method using very high pressure and very short sintering time was employed to avoid the grain growth usually observed during long-lasting high-temperature steps.

In this paper, we will first present our results concerning the synthesis of Ti/O/C nanopowders by laser pyrolysis and then

[†] DSM/DRECAM, CEA-Saclay.
[‡] Polish Academy of Sciences.
[§] SIFCOM-ENSICAEN.

10.1021/jp054471p CCC: $33.50 
Published on Web 12/09/2005

**TABLE 1: $TiO_xC_y$ Nanopowder Synthesis Conditions (Horizontal or Vertical Focalization, Nozzle Diameter ∅, and $C_2H_4$ and Ar Flows) and Properties (Ti, O, and C Contents, Free C Content $m_{fc}$)**

| sample name | lens | ∅ (mm) | $C_2H_4$ (sccm) | Ar (sccm) | Ti (wt %) | O (wt %) | C (wt %) | $m_c$(free) (wt %) |
|---|---|---|---|---|---|---|---|---|
| TiOC1 | horizontal | 6 | 1200 | 2000 | 53.8 ± 1.6 | 40.1 ± 1.2 | 6.1 ± 0.2 | 7.5 ± 0.2 |
| TiOC2 | vertical | 10 | 100 | 1100 | 40.7 ± 1.2 | 26.4 ± 0.8 | 32.8 ± 1.0 | 30.7 ± 0.6 |
| TiOC3 | vertical | 10 | 100 | 1035 | 39.8 ± 1.2 | 24.5 ± 0.7 | 35.6 ± 1.1 | 33.0 ± 0.7 |
| TiOC4 | vertical | 10 | 100 | 940 | 35.4 ± 1.1 | 24.9 ± 0.7 | 39.7 ± 1.2 | 37.3 ± 0.8 |

show the study concerning the carburization of these powders to form TiC nanoparticles. We will also present the results concerning the TiC nanostructured ceramics elaboration by high-pressure flash sintering.

## Experimental Section

The laser pyrolysis technique is based on the resonance between the emission of a $CO_2$ laser at 10.6 $\mu$m and the absorption of a gaseous or liquid precursor.[20] The experimental setup has been described elsewhere.[23] The confinement of the precursor flow by an argon chimney right at the exit of the inlet nozzle avoids any reaction with the reactor walls and protects the powders from any pollution. The chemical composition of the powders depends directly on the chemical composition of the precursor mixture. The short residence time of the radicals and particles in the hot zone induced by the laser beam limits the grain growth. The reaction time depends on this residence time, which mainly depends itself on the precursor mixture flow and on the nozzle diameter. The residence time can also be adjusted by the use of a lens that decreases the beam size above the nozzle.

For Ti/O/C synthesis, the liquid-phase titanium tetraisopropoxide $Ti(OC_3H_7)_4$ (TTIP) was supplied by Sigma-Aldrich (97% purity) and used without further purification. The aerosol was produced by an ultrasonic spraying technique (pyrosol process[24]) and carried into the reaction chamber by an Ar flow, allowing control of the amount of TTIP introduced into the reactor. Because this latter precursor weakly absorbs the laser radiation, ethylene $C_2H_4$ was added as a sensitizer gas because of its strong 10.6-$\mu$m absorption. A collisional energy transfer then takes place between $C_2H_4$ excited molecules and TTIP molecules, leading to the decomposition of the Ti precursor. Carrier Ar flow was varied between 300 and 2000 sccm, while $C_2H_4$ flow was varied in the 100−1200 sccm range. The laser power was kept constant at 690 W, and the beam was focused in a horizontal or vertical plane by means of a cylindrical lens. Two cylindrical nozzles were alternatively used, differing in their diameters ∅ (6 and 10 mm). When the diameter of the nozzle decreases, the velocity of the flow increases and, therefore, the time of residence in the laser beam decreases. After the synthesis, Ti/O/C powders were obtained with various contents of free C. They were then annealed in a graphite furnace during 1 h under an Ar atmosphere for various annealing temperatures $T_a$ to remove O and form TiC, as was already seen for Si/O/C reduction toward SiC in a previous work.[23]

The powders were characterized by different techniques. Chemical analyses were performed in CNRS Laboratory (Vernaison, France) in order to determine the composition of the $TiO_xC_y$ powders, with a relative uncertainty of 3%. The total C amount, which is in the present case, equivalent to the free carbon $m_c$(free) was determined by thermogravimetric analysis (TGA) by measuring the weight evolution after heat treatment. X-ray diffraction (XRD) patterns were obtained from a Philips X'Pert equipment using Cu K$\alpha_1$ radiation ($\lambda$ = 1.5406 Å). Crystallite sizes $T_{XRD}$ were subsequently calculated by Scherrer's method. The powders were also observed by means of field-emission scanning electron microscopy (SEM; LEO1530 apparatus), as well as transmission electron microscopy (TEM; Topcon 02B apparatus).

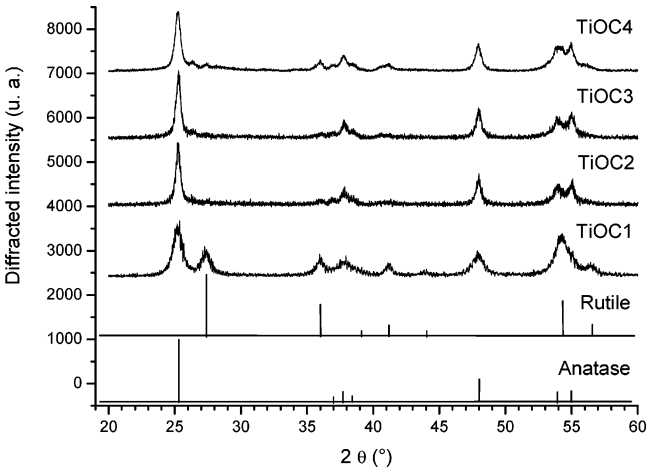


**Figure 1.** XRD diagrams recorded from TiOC1, TiOC2, TiOC3, and TiOC4 nanopowders together with references for rutile and anatase phases of $TiO_2$.

To elaborate nanostructured ceramics, TiC nanopowders were sintered without any additives by an original high-pressure flash method. The high-temperature step duration $t_s$ (up to a sintering temperature $T_s$ = 2000 °C) does not exceed 2 min in order to limit the grain growth. The pressure, which can reach $P_s$ = 8 GPa, is uniaxially applied by two WC specifically shaped anvils.[25] The starting powder is placed in a cylindrical BN container, which is itself placed inside a cylindrical graphite heater that is closed by two BN fillers. This assembly is placed in a $CaCO_3$ container, designed to fit the anvil profile, which somehow restores the pressure in every direction, making this method similar to conventional isostatic methods. For the samples presented in this paper, the following sintering parameters were used: $P_s$ = 8 GPa, $T_s$ = 1700 °C, and $t_s$ = 1 min. The sintered bodies were then examined by SEM and XRD, and their densities were measured by Archimedes' method.

## Results and Discussion

**(a) Ti/O/C Nanopowder Synthesis.** Several experimental conditions were tested to synthesize $TiO_xC_y$ nanopowders with $x$ and $y$ values enabling carburization (see section b) without any subsequent addition of C. The most representative conditions are summarized in Table 1, together with the powder composition. The mass of free C $m_c$(free), deduced from TGA measurements, can also be found in this table and compared with the C content measured by chemical analyses. These two measurements are generally close to each other. The slightly larger value given by chemical analyses is attributed to the presence of adsorbed species on the particle surface (water, precursor's residuals, hydrogenated carbons, etc.). The crystalline structure of the powders has also been investigated, and the XRD diagrams are presented in Figure 1. References for the anatase and rutile phases of $TiO_2$ are also given on this figure.

Two sets of experimental conditions can be distinguished in Table 1. The first one, concerning the TiOC1 sample, aims at the formation of very small Ti/O/C grains. Consequently, the horizontal focalization and the small nozzle were chosen to shorten the residence time of the reagents and particles in the laser beam (0.8 ms for TiOC1). The crystallite size is actually small ($T_{XRD} = 11.5 \pm 0.8$ nm for TiOC1), but the Ti chemical yield, defined as Ti collected in the powder divided by Ti introduced in the reaction zone, does not exceed 60%. Because of the short interaction time between the TTIP molecules and the laser beam, the Ti precursor is not well decomposed. This inefficient decomposition of TTIP leads to the adsorption of oxygenated species on the surface, which explains the high O content ($x = 2.2$). Despite the low chemical yield, the production rate is as high as 14 g·h$^{-1}$. Concerning now the C content, its low value can be explained by a weak decomposition of $C_2H_4$ for the same reason as that for TTIP. As one can see in Table 1, the $m_c$(free) value for sample TiOC1 is much too low to achieve complete carburization (see section b).

The second set of experiments, concerning TiOC2, TiOC3, and TiOC4 samples, was adjusted to achieve a better decomposition of TTIP and $C_2H_4$ than the one observed for TiOC1. The residence time was thus increased through the use of a wide nozzle in addition to a vertical focalization of the laser beam. The precursors and carrier flows were also decreased. In this case, the residence time reaches approximately 60 ms, which has to be compared to 0.8 ms of the first experiment. The decomposition is relatively efficient, with a Ti chemical yield of 84%. Consequently, there is less species coming from the incomplete decomposition of TTIP adsorbed on the surface, decreasing $x$ to approximately 2. The C content is higher than that in the first set, and this time the $m_c$(free) values are high enough to carburize the whole $TiO_2$. On the other hand, as a consequence of the longer residence time, the average crystallite size is around 25 nm (11.5 nm for TiOC1). The decrease of the carrier Ar flow leads to a lower amount of TTIP driven to the laser beam and therefore a lower production rate (7 g·h$^{-1}$ instead of 14 g·h$^{-1}$ for TiOC1).

Figure 1 shows that the only crystalline phase in the powder is $TiO_2$, mainly in its anatase phase. Nevertheless, a strong rutile contribution is observed in the TiOC1 sample. This can be related to the high $C_2H_4$ flow used for the synthesis of this latter sample, leading to a strong absorption of the laser power (190 W for TiOC1 instead of ~60 W for the other samples). Consequently, the flame temperature is higher than the one encountered in the case of weak absorption. It appears therefore that, although the dissociation of TTIP is globally less efficient because of the short time of residence, these high-temperature reaction conditions allow the formation of the high-temperature phase of $TiO_2$(rutile). Moreover, no suboxide or carbide phase can be observed in any sample. Taking all of these results into consideration, we assume that independently of our synthesis conditions the value of $x$ in our $TiO_xC_y$ powders is always very close to 2.

**(b) TiC Nanopowder Formation after Carburization.** Let us first recall the reaction ruling the carburization process:

$$TiO_2 + 3C \rightarrow TiC + 2CO \quad (1)$$

To complete such a reaction with stoichiometric $TiO_2$, a total amount of free C $m_c$(free) = 31.1 wt % is needed, and the consecutive weight loss after carburization will be $m_L = 48.3$ wt %.

To find the lowest annealing temperature $T_a$ needed to complete the carburization reaction ruled by eq 1, the TiOC4 sample was submitted to a heat treatment in a graphite furnace under an Ar atmosphere for 1 h at different values of $T_a$ in the 1000−1500 °C range. Figure 2 shows XRD patterns obtained from TiOC4 nanopowder, as synthesized and after the annealing treatment at $T_a = 1000$, 1200, 1250, and 1300 °C. The powder characteristics (mass loss $m_L$ and cell parameter $a$) after annealing are reported in Table 2.

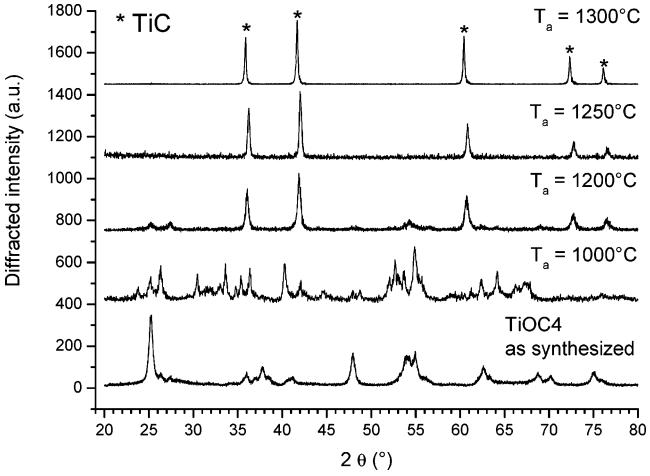


**Figure 2.** XRD diagrams from the TiOC4 nanopowder as synthesized and after annealing under argon for 1 h at the indicated temperatures.

**TABLE 2: TiOC4 Nanopowder Characteristics after 1 h of Annealing under Argon at the Indicated Annealing Temperatures $T_a$ (Mass Loss $m_L$ and Cell Parameter $a$)**

| $T_a$ (°C) | $m_L$ (wt %) | $a$ (Å) |
|---|---|---|
| 1200 | 29.7 ± 1.0 | 4.296 ± 0.005 |
| 1250 | 40.1± 1.5 | 4.310 ± 0.005 |
| 1300 | 44.4± 1.5 | 4.331 ± 0.005 |

As has already been seen in Figure 1, no TiC phase can be observed in the as-synthesized powder in Figure 2. Concerning the lowest annealing temperature ($T_a = 1000$ °C), one can notice that the anatase phase transformation toward the rutile phase, mixed with a slight contribution of suboxide phases, is ignited. It is worth noticing that 1000 °C is a quite low temperature to begin the carbothermal reduction because the carbothermal reduction of raw $TiO_2$ materials by carbon black is known to begin at 1200 °C.[26] The formation of suboxide phases ($Ti_4O_7$, $Ti_3O_5$, and $Ti_2O_3$) during the carburization process has already been reported.[17,27]

For $T_a = 1200$ °C, the oxide peaks decrease while new diffraction peaks appear close to the position of the TiC phase peaks, though they are slightly shifted toward larger angles. Indeed, the cell parameter value $a = 4.296 \pm 0.005$ Å calculated from this diagram (cf. Table 2) is smaller than the one for pure TiC ($a = 4.3280$ Å[28]). Such low values can be related to the presence of O in TiC as a solid solution of TiO in TiC, giving an oxycarbide phase.[29] Similar values of $a$ have already been reported and attributed to an oxycarbide phase $Ti_2OC$ ($a = 4.2960$ Å).[30] The low mass loss $m_L$ value recorded (cf. Table 2) after the $T_a = 1200$ °C annealing treatment ($m_L = 29.7 \pm 1.0$ wt %) confirms, when compared to $m_L = 48.3$ wt % given by eq 1, that the carburization was not complete and thus allowed some unreduced O in the powder.

The oxycarbide phase still remains at $T_a = 1250$ °C, while the oxide phases are no longer there. This observation is confirmed by the values of $m_L$ and $a$ (cf. Table 2), although these parameters are getting closer to their theoretical and reference values for TiC formation.

**TABLE 3: TiC2, TiC3, and TiC4 Nanopowder Characteristics after 1 h of Annealing under Argon at $T_a = 1300$ °C of the TiOC2, TiOC3, and TiOC4 Samples, Respectively [Mass Loss $m_L$; TiC Cell Parameter $a$; TiC Crystallite Size $T_{XRD}$; Ti, C, and O Contents; and $TiC_w(O_z)$ Formula]**

| sample | $m_L$ (wt %) | $a$ (Å) | $T_{XRD}$ (nm) | Ti (wt %) | C (wt %) | O (wt %) | $TiC_w(O_z)$ |
|---|---|---|---|---|---|---|---|
| TiC4 | 44.4 ± 1.5 | 4.331 ± 0.005 | 82.0 ± 5.7 | | | | |
| TiC3 | 47.1 ± 1.5 | 4.323 ± 0.005 | 86.6 ± 6.1 | 68.3 ± 2.1 | 26.7 ± 0.8 | 4.9 ± 0.2 | $TiC_{1.56}(O_{0.22})$ |
| TiC2 | 47.1 ± 1.5 | 4.317 ± 0.005 | 75.9 ± 5.3 | 72.7 ± 2.2 | 21.5 ± 0.6 | 5.8 ± 0.2 | $TiC_{1.18}(O_{0.24})$ |

Finally, for $T_a = 1300$ °C, the cell parameter value reaches $a = 4.3301 \pm 0.005$ Å, giving evidence for pure TiC formation. The complete carburization is confirmed by the $m_L$ value, in acceptable agreement with that of eq 1 even though it is a little lower. Indeed, for $T_a = 1500$ °C (not shown here), the recorded values for $a$ and $m_L$ were the same as those for $T_a = 1300$ °C. The difference between the theoretical value of $m_L$, calculated from eq 1 ($m_L = 48.3$ wt %), and the observed one for $T_a = 1300$ °C can be attributed to a slight reduction of $TiO_2$ during the synthesis ($x < 2$). This temperature is quite lower than the one usually encountered in carbothermal reduction in industrial processes (>1700 °C[14]) and equivalent to the ones observed with other carburization routes.[18,19] The final TiC mean crystallite size for $T_a = 1300$ °C can then be estimated as $T_{XRD} = 82.0 \pm 5.7$ nm, with a starting $TiO_2$ crystallite size of about 25 nm. If we manage to decrease this latter $TiO_2$ size, together with keeping the right $x$ and $y$ values in $TiO_xC_y$ to complete the carburization process, we should be able to decrease both the annealing temperature and the final TiC crystallite size.

Figure 3 shows a SEM picture of the TiC4 nanopowder (TiOC4 powder after annealing at 1300 °C). One can notice that the grain size distribution appears to be homogeneous and close to the mean crystallite size ($T_{XRD} = 82.0$ nm) even if few smaller grains can be observed. Moreover, the grain shape appears to be not round but faceted. This is an indication that the TiC grains are monocrystalline. Figure 4 presents a high-resolution TEM image of the same sample; it clearly shows that the grains are monocrystalline. One can also notice that the grains are coated by free C because of the excess C in the as formed TiOC4 powder. The free C content was indeed $m_c$-(free) = 37.3 ± 0.8 wt %, instead of the 31.1 wt % needed to satisfy eq 1. The free C excess in the final TiC4 powder can thus be estimated as ~14 wt %.

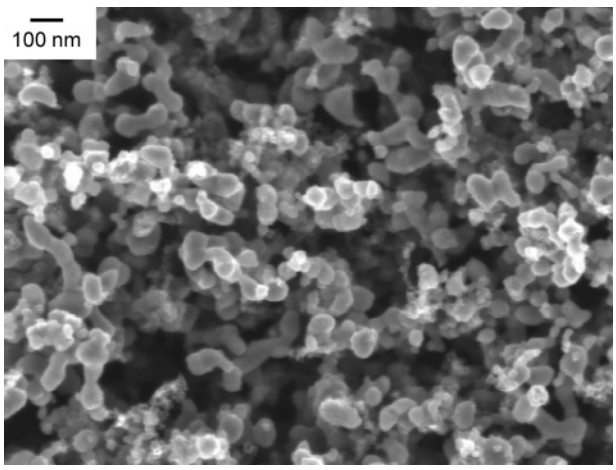


**Figure 3.** SEM picture showing TiC nanograins (TiC4 sample), recorded from the TiOC4 nanopowder after annealing for 1 h under argon at $T_a = 1300$ °C.

TiOC2 and TiOC3 samples were submitted to the same annealing treatment as TiOC4 ($T_a = 1300$ °C). The characteristics of the carburized samples TiC2 and TiC3 are summarized in Table 3 in comparison with those of TiC4.

Once again the annealing treatment led to the formation of the TiC phase. Nevertheless, one can notice a small decrease in the $a$ values, together with an increase in the O content, with a decrease of the C content. This could be attributed to an easier oxidization in the ambient atmosphere of the TiC2 and TiC3 samples, which are less protected than TiC4 from air by a free carbon shell. After a 1500 °C annealing step, the recorded values for $a$ and $m_L$ were the same as those after the 1300 °C treatment, as was already observed for the TiC4 sample.

A SEM picture of the TiC2 sample can be seen in Figure 5. It appears that the size distribution is wider than it was for the free-C-rich sample. Indeed, one can observe small (<40 nm) and large grains (>120 nm) even if the average crystallite size is close to the one calculated for TiC4 (cf. Table 3). We assume that this is due to the coalescence between some growing grains during the annealing treatment. This phenomenon did not occur in the TiC4 sample because of the large amount of free C coating the grains and thus inhibiting the coalescence.

**(c) Nanostructured Ceramics Elaboration.** To elaborate nanostructured ceramics, the TiC4 nanopowder was sintered by the high-pressure flash-sintering method. The high free C content in the TiC4 powder hardly allows a direct comparison with the TiC theoretical density (4.93). Nevertheless, the sintered bodies showed a relatively high density (3.90) if one takes into account

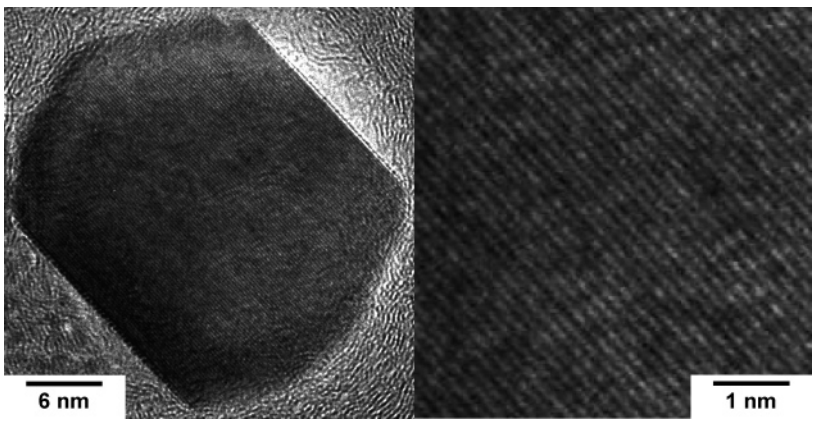


**Figure 4.** TEM picture showing one small TiC grain, recorded from a free-C-rich TiC4 nanopowder. The right part of the figure shows a magnification of the left part.

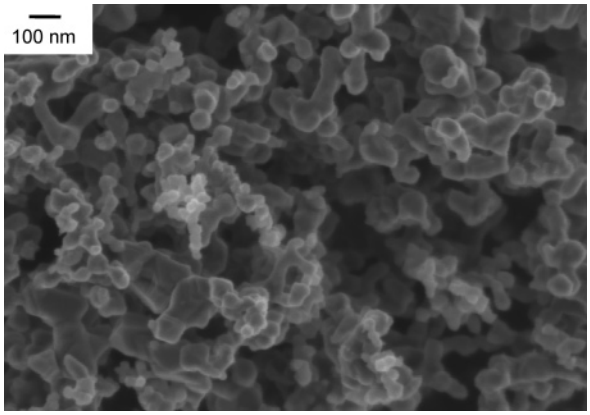


**Figure 5.** SEM picture recorded from the TiC2 sample.

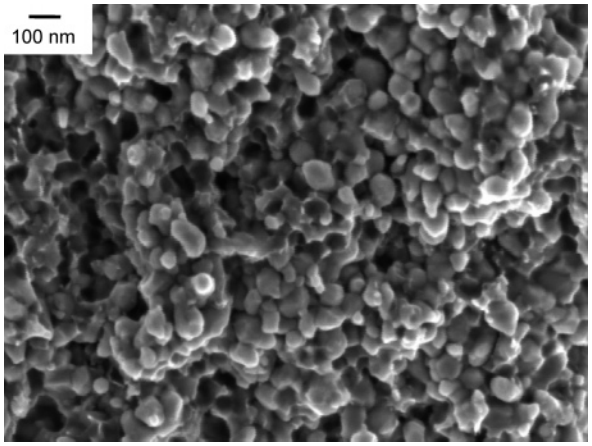


**Figure 6.** SEM picture recorded on TiC4 after sintering ($P_s = 8$ GPa, $T_s = 1700$ °C, and $t_s = 1$ min).

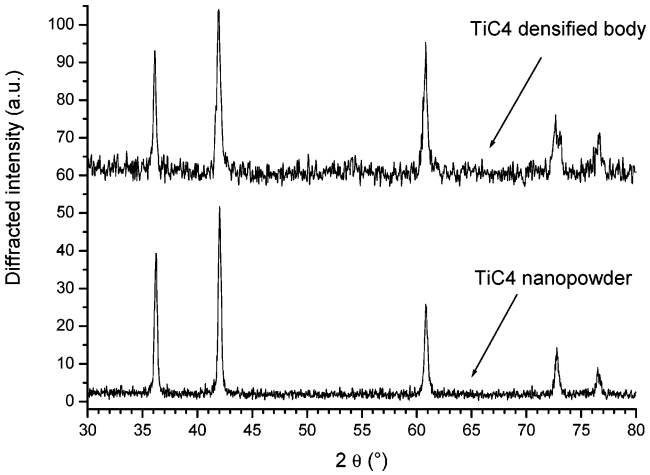


**Figure 7.** XRD diagrams recorded from the TiC4 nanopowder, before and after sintering ($P_s = 8$ GPa, $T_s = 1700$ °C, and $t_s = 1$ min).

the high C content. For the TiC4 sample, the densification was thus $d = 79\%$. This low value can be attributed to the high free C content that inhibits the cohesion between the grains. The shape and size of the grains after sintering appear very similar to what they were before, as one can notice by comparing Figure 6, which presents a SEM picture recorded from the sintered TiC4 sample, with Figure 3. This observation is confirmed by the XRD diagrams shown in Figure 7, recorded from the TiC4 sample before and after sintering. One can even notice that a tiny broadening of the peak occurs after sintering, giving evidence of weak stress within the pellet.

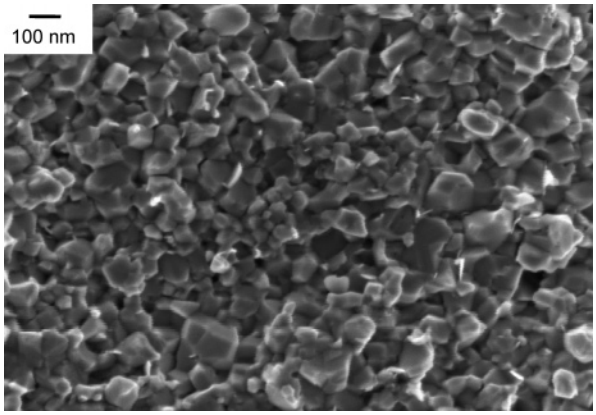


**Figure 8.** SEM picture recorded from the TiC2 sample after sintering ($P_s = 8$ GPa, $T_s = 1700$ °C, and $t_s = 1$ min).

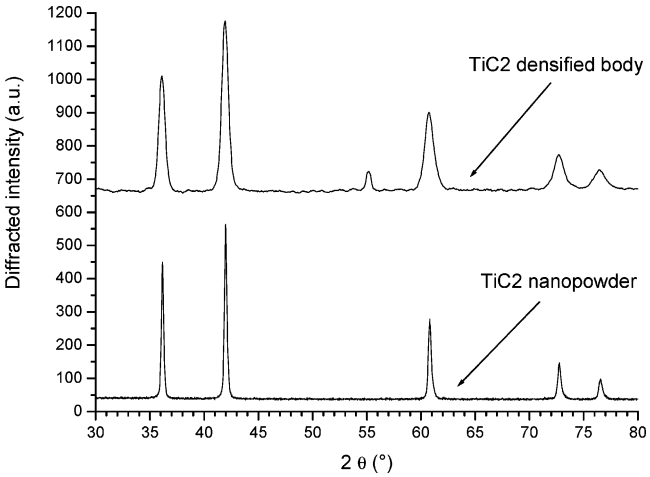


**Figure 9.** XRD diagrams recorded from the TiC2 nanopowder, before and after sintering ($P_s = 8$ GPa, $T_s = 1700$ °C, and $t_s = 1$ min).

The same sintering process was applied to the TiC2 sample in order to study the behavior of quasi-stoichiometric TiC. SEM observation was achieved on a sintered TiC2 sample and is presented in Figure 8. Even for this sample, where there is no free C to play a key role during the sintering process, the grain size remained as small as it was before sintering (cf. Figure 5), and the dispersion in the size distribution can still be observed. The hypothesis concerning the inhibition of the grain growth by free C can thus be abandoned, and the absence of grain growth can then be exclusively attributed to the very short duration of the high-temperature step during sintering. The absence of grain growth is confirmed by the XRD diagrams shown in Figure 9, where once again there is a broadening of the diffraction peaks during the sintering. Comparing to what was observed with the TiC4 sample, the broadening that can be seen in Figure 9 is stronger and lets one think that the TiC2 pellet is more stressed than the TiC4 one. We assume that in the case of the free-C-rich sample the stress is somehow released in the intergranular layers of C.

Furthermore, the density measurements performed on the TiC2 sintered pellet showed an acceptable densification $d = 93\%$. This improvement of the densification can be related, on the one hand, to a better cohesion between the grains because of the low free C content and, on the other hand, to the wide size distribution, including small and large grains, known to improve the compaction.

## Conclusion

We achieved the synthesis of nanosized monocrystalline TiC powders through the carburization of Ti/O/C nanopowders grown by laser pyrolysis from easy-to-use cheap precursors. No subsequent C addition was needed to obtain the complete reduction of the oxide phase because the composition of the Ti/O/C as-synthesized mixture was successfully controlled. We also managed to decrease the carbothermal reduction process temperature because the annealing temperature needed to complete the carburization process was found to be as low as 1300 °C, with a final TiC crystallite and grain size of about 80 nm. This work has also demonstrated the possibility of obtaining a satisfying densification of the ceramics pellet by the high-pressure flash-sintering method ($d$ = 93%), together with avoiding the grain growth to conserve the nanometric structure. The presence of free C was found to lower the densification but also to protect the carbide powders from oxidization in air. The optimization of the synthesis process is now addressed to obtain the direct formation of carbide powders without any annealing posttreatment. Concerning the Ti/O/C powders, our study is now focused on the decrease of the $TiO_2$ particle size, together with keeping accurate control of the chemical composition. In parallel with the high-pressure flash-sintering study that will go on, other ceramics elaboration techniques will be considered, such as the spark plasma sintering method. The elaboration of larger pellets will also be addressed in order to enable mechanical property characterization tests.

**Acknowledgment.** The authors thank Marie-Noelle Metzner (SIFCOM) for XRD measurements. This collaboration was supported by an “action intégrée” Polonium.

## References and Notes

(1) Hintermann, H. E. *Wear* **1984**, *100* (1−3), 381.
(2) Gross, V.; Haylock, J.; Swain, M. V. *Mater. Sci. Forum* **1988**, *34*−*36*, 555.
(3) Mei, Z.; Yan, Y. W.; Cui, K. *Mater. Lett.* **2003**, *57*, 3175.
(4) Kim, Y. W.; Lee, S. G.; Lee, Y. I. *J. Mater. Sci.* **2000**, *35*, 5569.
(5) Chae, K. W.; Niihara, K.; Kim, D. Y. *J. Mater. Sci. Lett.* **1995**, *14*, 1332.
(6) Endo, H.; Ueki, M.; Kubo, H. *J. Mater. Sci.*, **1991**, *26*, 3769.
(7) Vassen, R.; Stöver, D. *Mater. Sci. Eng. A* **2001**, *301*, 59.
(8) Vassen, R.; Kaiser, A.; Stöver, D. *J. Nucl. Mater.* **1996**, *233*−*237*, 708.
(9) Dutremez, S.; Gerbier, P.; Guérin, C.; Henner, B.; Merle, P. *Adv. Mater.* **1998**, *10* (6), 465.
(10) Lee, D. W.; Alexandrovskii, S. V.; Kim, B. *Mater. Lett.* **2004**, *58*, 1471.
(11) Pierson, H. O. In *Handbook of refractory carbides and nitrides*; Noyes Publications: Park Ridge, NJ, 1996.
(12) Tong, L.; Reddy, R. G. *Scr. Mater.* **2005**, *52*, 1253.
(13) Miracle, D. B.; Lipsitt, H. A. *J. Am. Ceram. Soc.* **1983**, *66*, 592.
(14) Thorne, K.; Ting, S.; Chu, C. J. *J. Mater. Sci.* **1992**, *27*, 4406.
(15) Hassine, N. A.; P. Binner, J. G.; Cross, T. E. *Int. J. Refract. Met. Hard Mater.* **1995**, *13*, 353.
(16) Koc, R.; Folmer, J. S. *J. Mater. Sci.* **1997**, *32*, 3101.
(17) Lefort, P.; Maitre, A.; Tristant, P. *J. Alloys Compd.* **2000**, *302*, 287.
(18) Swift, G. A.; Koc, R. *J. Mater. Sci.* **1999**, *34*, 3083.
(19) Gotoh, Y.; Fujimura, K.; Koike, M.; Ohkoshi, Y.; Nagura, M.; Akamatsu, K.; Deki, S. *Mater. Res. Bull.* **2001**, *36*, 2263.
(20) Cannon, W. R.; Danforth, S. C.; Flint, J. H.; Haggerty, J. S.; Marra, R. M. *J. Am. Ceram. Soc.* **1982**, *65* (7), 324.
(21) Cauchetier, M.; Croix, O.; Luce, M. *Adv. Ceram. Mater.* **1988**, *3* (6), 548.
(22) Alexandrescu, R.; Borsella, E.; Botti, S.; Cesile, M. C.; Martelli, S.; Giorgi, R.; Turtu, S.; Zappa, G. *J. Mater. Sci.* **1997**, *32*, 5629.
(23) Herlin, N.; Armand, X.; Musset, E.; Martinengo, H.; Luce, M.; Cauchetier, M. *J. Eur. Ceram. Soc.* **1996**, *16*, 1063.
(24) Langlet, M.; Joubert, J. C. Blackwell Scientific Publications: 1992; p 55.
(25) Khvostantsev, L. G.; Vereshchagin, L. F.; Novikov, A. P. *High Temp.-High Pressures* **1977**, *9*, 637.
(26) Licko, T.; Figusch, V.; Puchyova, J. *J. Eur. Ceram. Soc.* **1989**, *5*, 257.
(27) Koc, R. *J. Mater. Sci.* **1998**, *33*, 1049.
(28) Storms, E. K. *The Refractory Carbides*; Academic Press: New York, 1967.
(29) Preiss, H. E.; Schierhorn, K.; Brzezinka, W. *J. Mater. Chem.* **1998**, *33*, 4697.
(30) Ivanov, N. A.; Andreeva, L. P.; Gel’d, P. V. *Sov. Powder Met. Ceram.* **1978**, *17*, 613.